

Supplement of

High-resolution mapping of vehicle emissions of atmospheric pollutants based on large-scale, real-world traffic datasets

5 Daoyuan Yang ^{1, #}, Shaojun Zhang ^{2, #}, Tianlin Niu ^{1, 3}, Yunjie Wang ¹, Honglei Xu ⁵, K. Max Zhang ²,
Ye Wu ^{1, 4, *}

¹School of Environment, State Key Joint Laboratory of Environment Simulation and Pollution Control, Tsinghua University, Beijing 100084, P R China.

²Sibley School of Mechanical and Aerospace Engineering, Cornell University, Ithaca, NY 14853, U.S.A.

³Ricardo Energy & Environment, Beijing 100028, P R China.

10 ⁴State Environmental Protection Key Laboratory of Sources and Control of Air Pollution Complex, Beijing 100084, P R China.

⁵Transport Planning and Research Institute, Ministry of Transport, Beijing 100028, PR China

* *Correspondence to:* Y. Wu (ywu@tsinghua.edu.cn)

These authors contributed equally to this paper.

15

Summary of Supplementary Information:

Part I. Supplementary tables and figures

Part II. Generating dynamic traffic profiles based on congestion information

20 Part III. Simulating vehicular NO_x concentrations by using the RapidAir® model

Part IV. Comparing emission inventories based on link-level traffic data and top-down allocation methods

Supplementary Figures

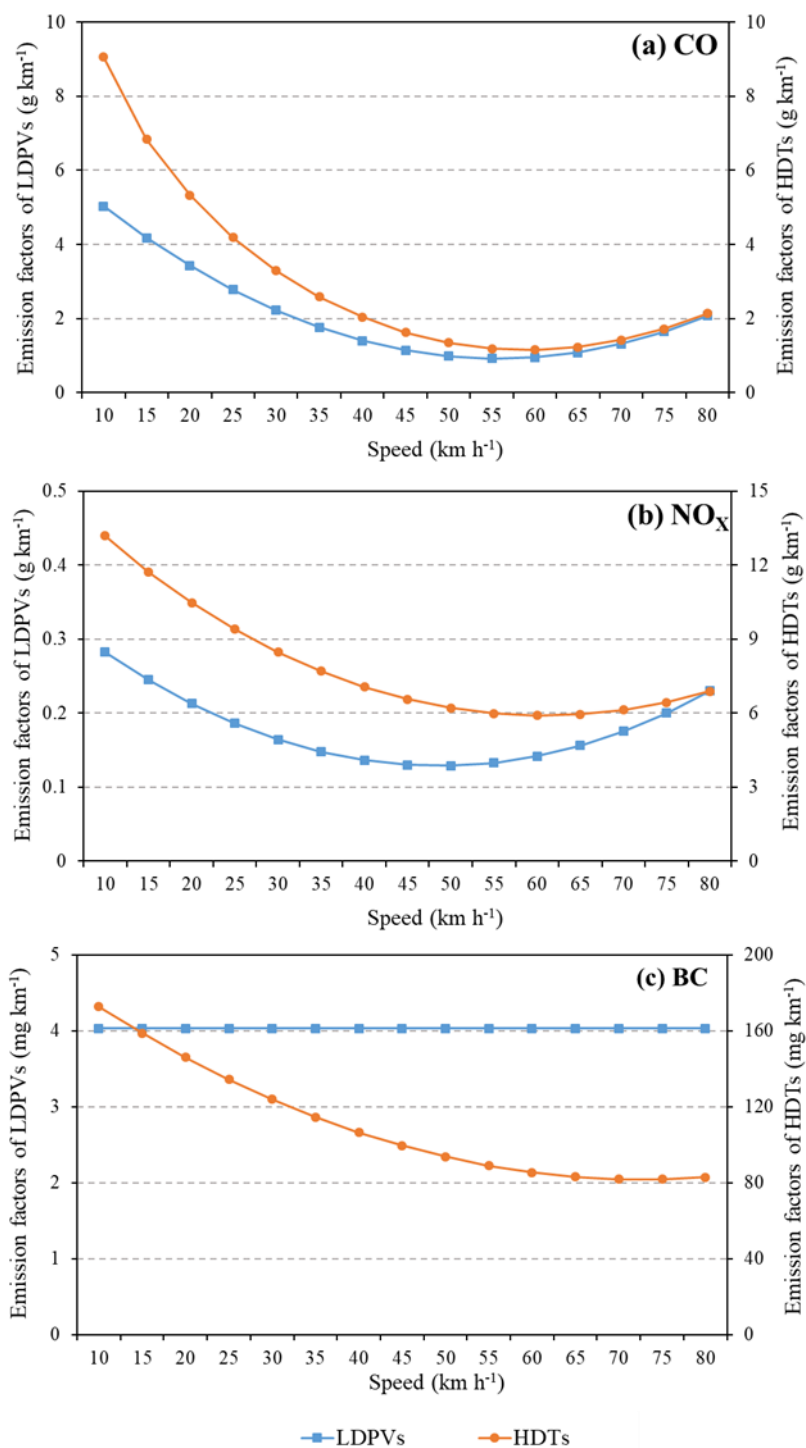


Figure S1. Speed-dependent fleet-average emission factors for LDPVs and HDTs: (a) CO, (b) NO_x and (c) BC

Note: Speed correction is not applicable to BC emissions from LDPVs due to the lack of testing data

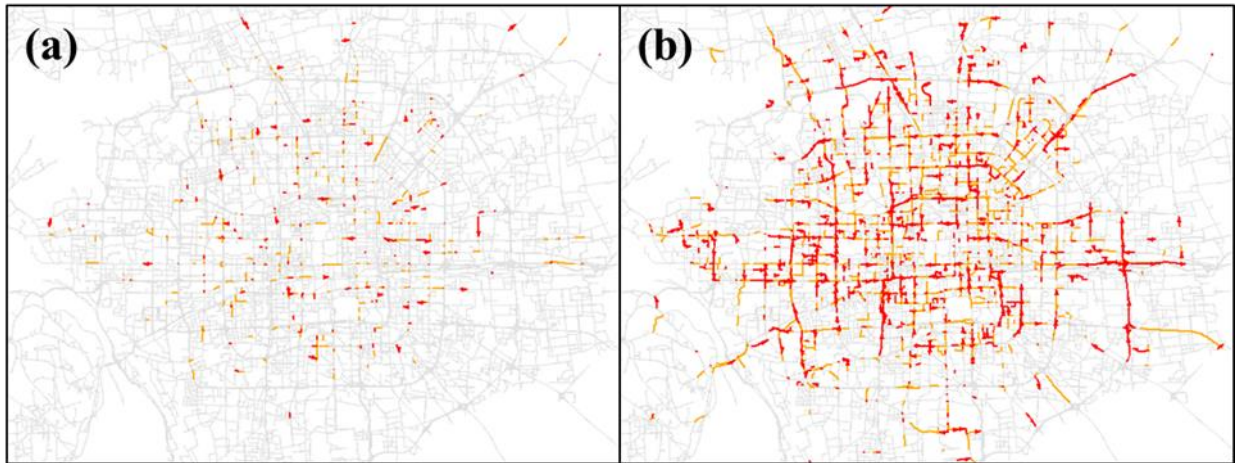


Figure S2. Examples of color-informed congestion index maps: (a) nighttime period (0:00 GMT+8) and (b) morning peak period (7:00 GMT+8).

Note: The maps cover the entire area within the Sixth Ring Road, but most of the available data were obtained from the area within the Fifth Ring Road (i.e., the urban area).

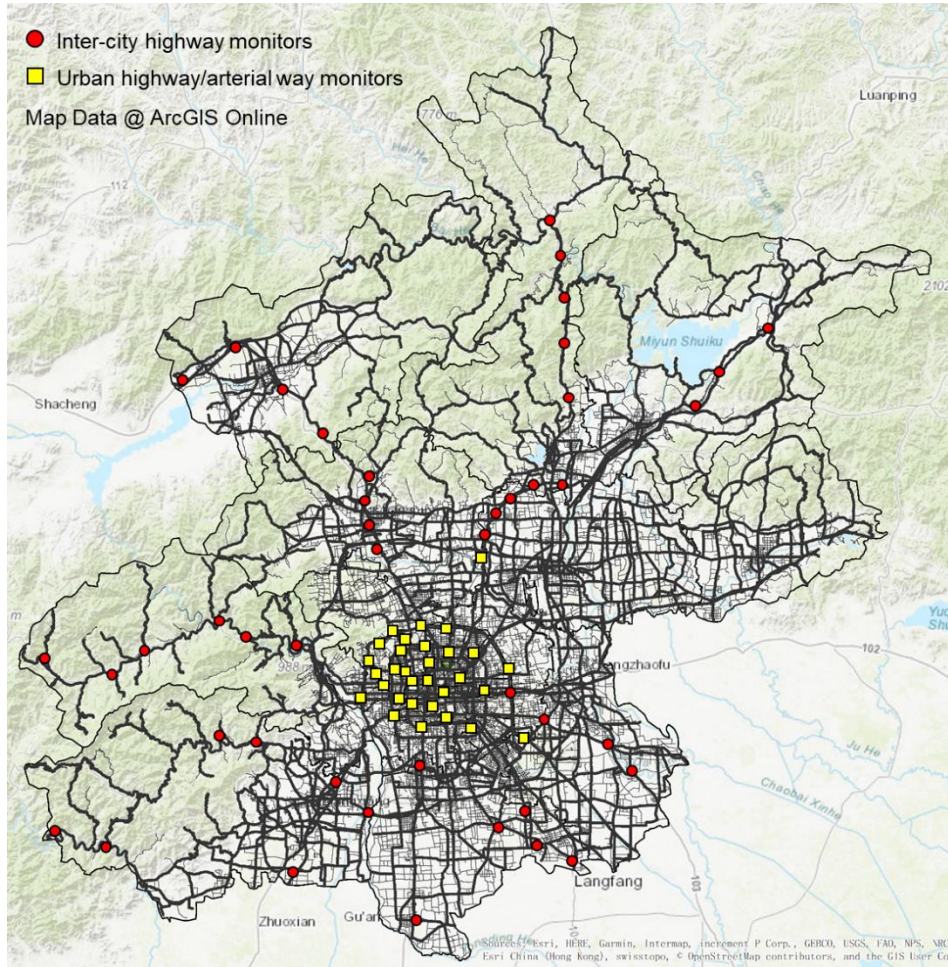


Figure S3. Map of traffic monitoring sites with traffic mix data available.

Note: The red markers indicate the inter-city highway traffic monitoring sites, which generate detailed observations for total volume, fleet mix and road speed and report to the Ministry of Transport (MOT) of China. The yellow markers represent the sites with traffic video records, which were conducted by researchers from Tsinghua University.

40

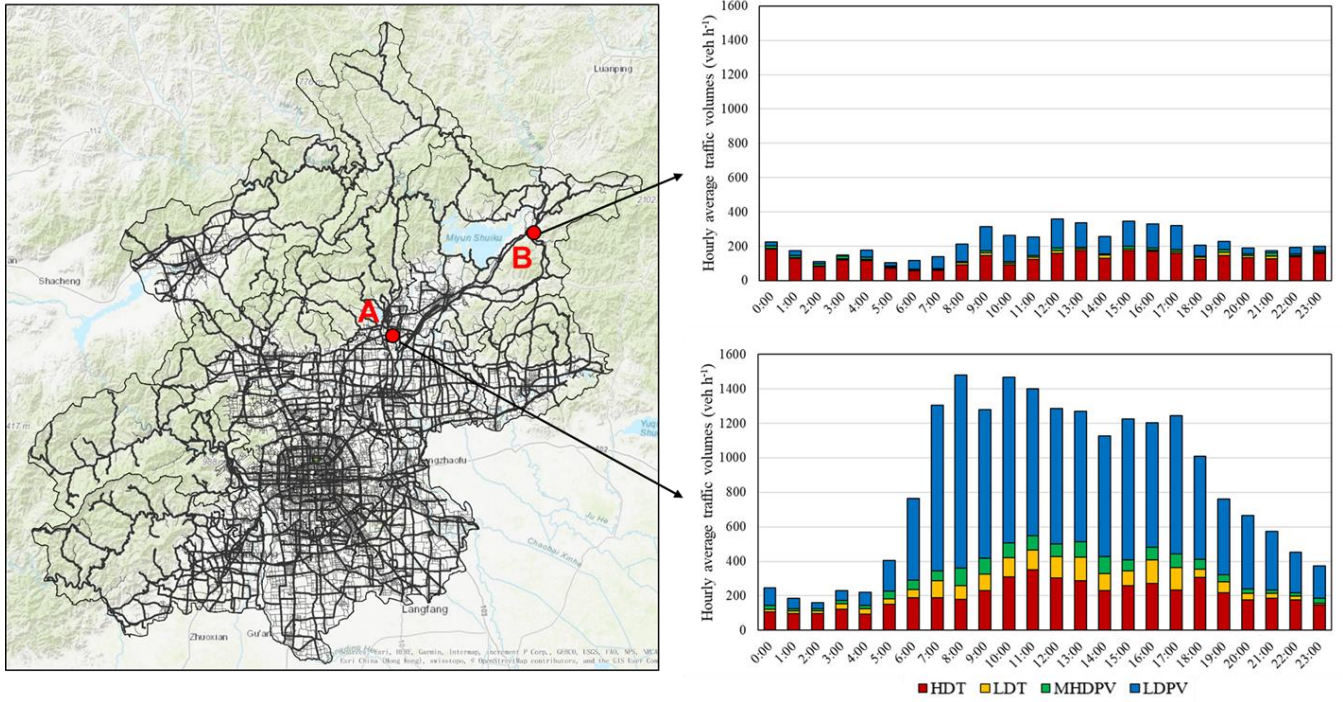
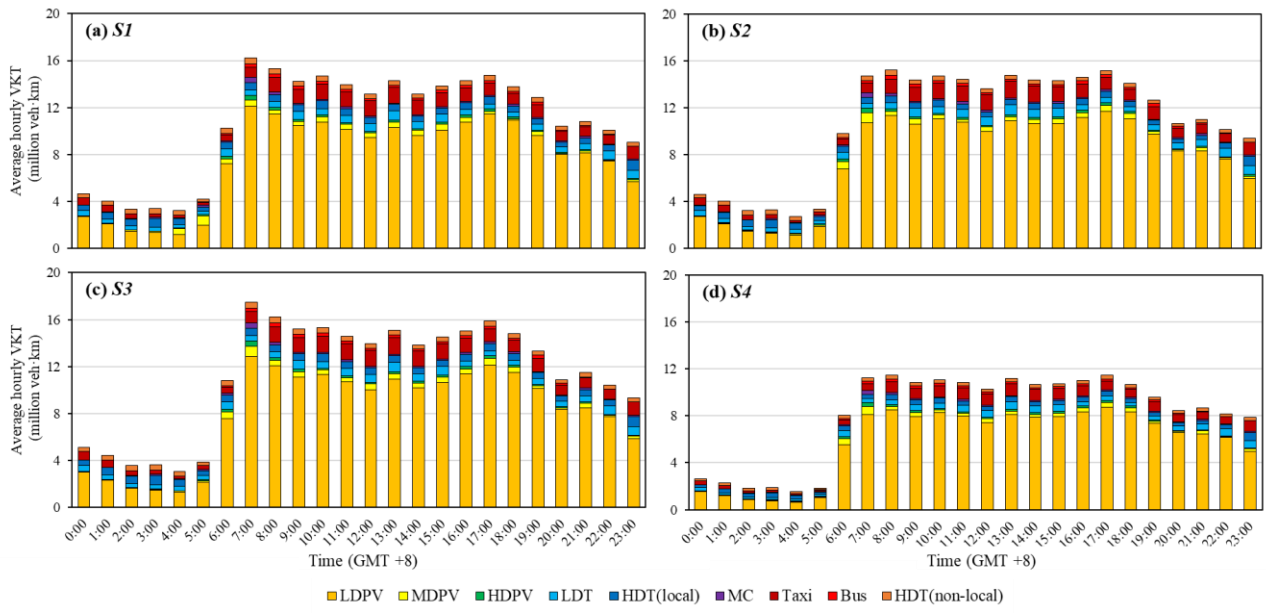


Figure S4. Map of inter-city highway traffic monitoring sites in Beijing. Sites A (close to the Fifth Ring Road) and B (close to the city border of Beijing) represent two monitoring locations along Expressway G101.



45 **Figure S5. Diurnal fluctuations in hourly traffic activity by vehicle category during various traffic scenarios *S1* to *S4*.**

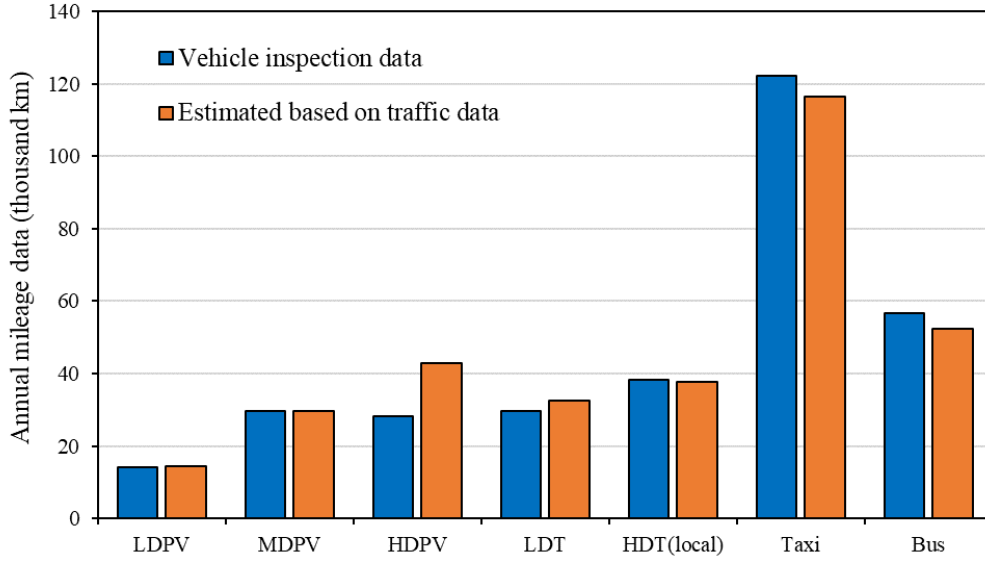


Figure S6. Comparison of the annual mileage data between the estimated results and registered data.

Note: The vehicle inspection dataset includes vehicle mileage records, and we obtained the processed data from local environmental protection authorities to represent the fleet-average annual vehicle kilometer travelled (VKT) (Zhang et al., 2014). The traffic volume informed annual VKT is estimated according to Eq. (S1) (Zhang et al., 2018).

$$\overline{VKT}_{traffic,c} = \frac{365 \cdot \sum_{h,l} L_l \cdot (\overline{TV}_{c,h,l})}{P_c}$$

(S1)

where $\overline{VKT}_{traffic,c}$ is fleet-average annual traffic VKT for vehicle category c , km; $\overline{TV}_{c,h,l}$ is the average traffic volume for vehicle category c , hour h and road link l , veh, which is weighted by various traffic scenarios (e.g., weekday, weekend); P_c is total population for category c that are issued with Beijing license plates, veh.

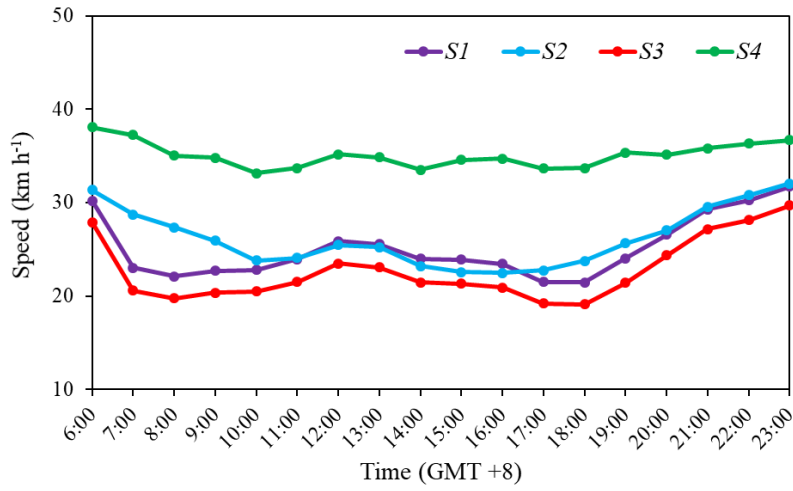
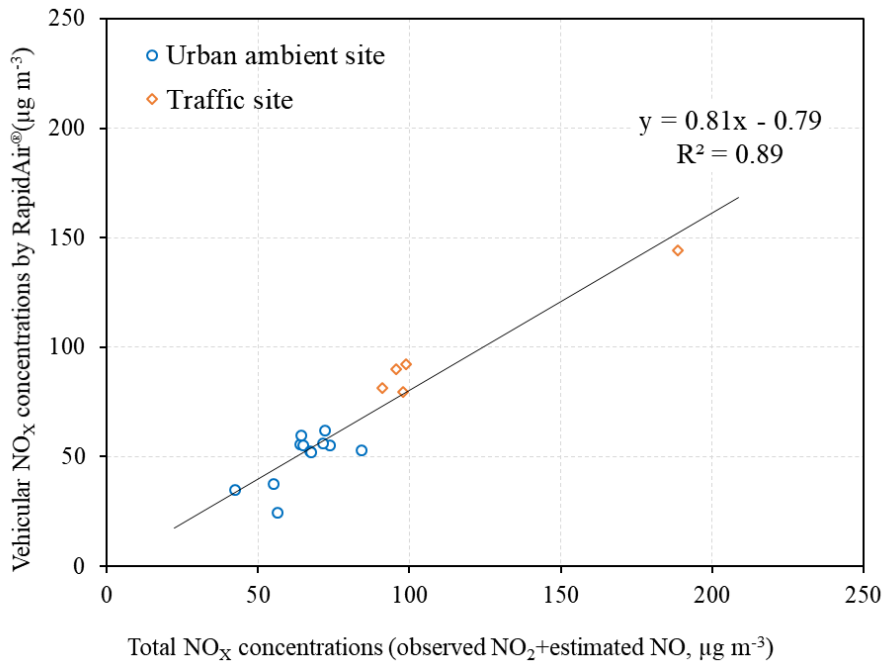


Figure S7. Average hourly speed of the area within the Fifth Ring Road under various traffic scenarios.



60 **Figure S8. The daytime comparison of average vehicular NO_x concentrations and total NO_x concentrations for all the urban and traffic sites in Beijing, 2013.**

Note: The site-specific daytime NO concentration (6:00 to 17:00 GMT+8) is estimated according to the average NO₂ and O₃ concentrations, which is documented in Supplementary Information Part III. The observed NO₂ and O₃ concentrations were downloaded via the Beijing Environmental Protection Bureau (Now Beijing Municipal Ecological Environment Bureau).

65

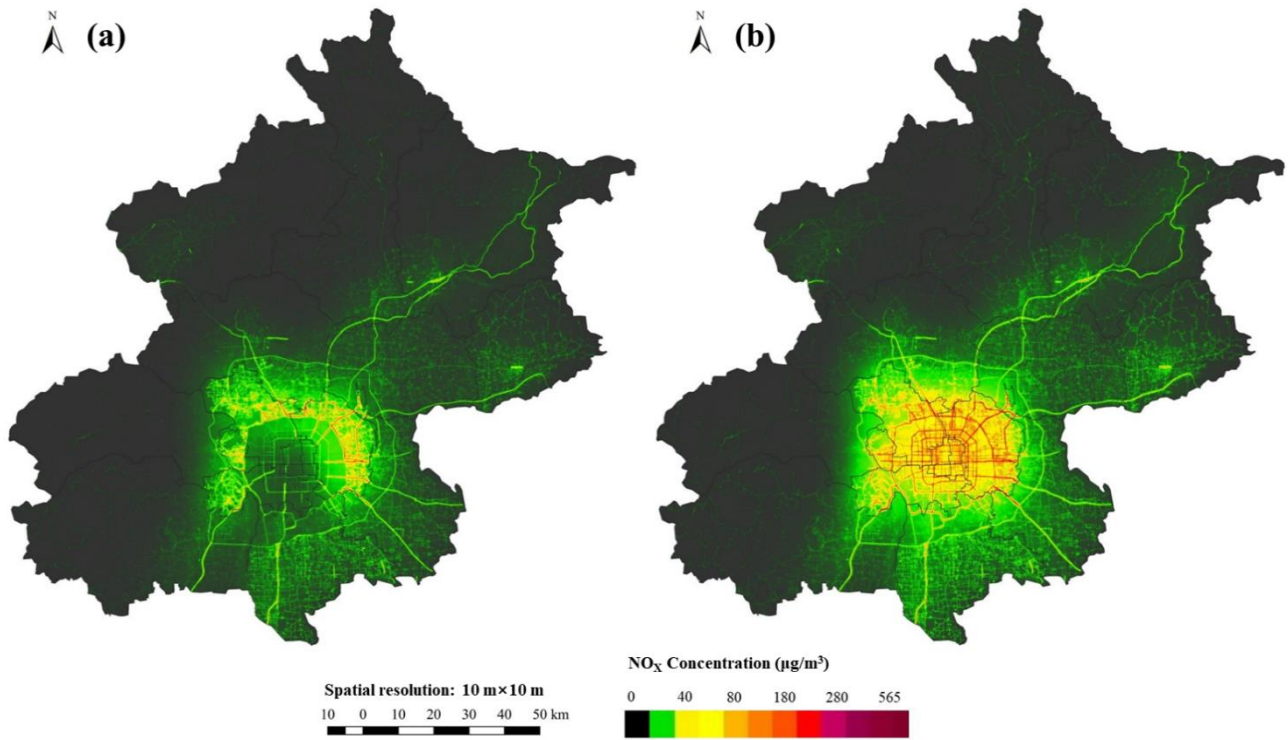


Figure S9. The simulated NO_x concentrations contributed by HDTs: a) the daytime (average from 6:00 to 22:00 GMT+8) and b) the nighttime (from 23:00 to 6:00 GMT+8).

Table S1. Definition and abbreviation of vehicle categories

| Vehicle classification | Abbreviation | Description |
|-------------------------------|--------------|----------------------------|
| Light-duty passenger vehicle | LDPV | PC ^a ≤ 9 |
| Medium-duty passenger vehicle | MDPV | 9 < PC ≤ 20 |
| Heavy-duty passenger vehicle | HDPV | PC > 20 |
| Light-Duty Truck | LDT | GVW ^b ≤ 4500 kg |
| Heavy-Duty Truck ^c | HDT | GVW > 4500 kg ^d |
| Public Bus | Bus | |
| Taxi | Taxi | |
| Motorcycle | MC | |

Notes: ^a Passenger capacity; ^b Gross vehicle weight; ^c The HDTs are further classified into local HDTs and non-local HDTs according to the registration place; ^d The GVW values of non-local HDTs are mostly above 12000 kg, which use the emission factors of HDT3 (GVW > 12000 kg) estimated by Wu et al. (2012) (Wu et al., 2012). By contrast, emission factor for local HDTs are weighted by HDT2 and HDT3 according to their registration number and annual VKT (Zhang et al., 2014).

Table S2. Major traffic management schemes under various traffic scenarios

| Scenario | Relevant vehicle category | | |
|---------------|---|---|--|
| | LDPVs | Local HDTs | Non-local HDTs |
| S1-Weekday | Regular restrictions by stopping one weekday (from 7:00 to 22:00 GMT+8) per week within the Fifth Ring Road. | HDTs have been only allowed to drive within the Fourth Ring Road from 23:00 to 6:00 (GMT+8) since 2004, and the restrictive boundary has been expanded to the Fifth Ring Road (not including the Fifth Ring Road) since April 2014. | Non-local HDTs have been only allowed to drive within the Fifth Ring Road from 0:00 to 6:00 (GMT+8), and the restrictive boundary has been extended to the Sixth Ring Road since April 2014. |
| S2-Weekend | No regular restrictions. | In particular, HDTs with GVW over 8 tons have been prohibited from the main segment of Fifth Ring Road from 6:00 to 23:00 since April 2014 (previously 6:00 to 22:00 GMT+8). | |
| S3-Congestion | No regular restrictions. | | |
| S4-APEC | 70% of government-owned vehicles were controlled off road. | HDTs were only allowed to drive within the Sixth Ring Road from 0:00 to 6:00 (GMT+8) | Non-local HDTs were not allowed to drive within the Sixth Ring Road all day around. |
| | Odd-even driving restrictions were implemented from 3:00 to 0:00 (GMT+8) for all the vehicles in the entire city, and especial public and municipal fleets were exempted. | | |

Part II. Generating high-resolution traffic profiles

2.1 Calculating hourly road speeds based on real-time traffic congestion index data

According to the official guideline of congestion index (Beijing Municipal Administration of Quality and Technology Supervision and BTI, 2011), the index ranges from 0 to 5 representing more serious levels of congestion. Table S3 summarizes the relationship between color indicator, congestion index range and speed interval by road type. For example, grey indicate a congestion index below 3, representing average speed greater than 20 km/h for arterial roads. We proposed quadratic functions to express the relationship between congestion index and road speed and used breakpoints in Table S3 as known data for function fitting (see Fig. S10). For example, the data pairs (*congestion index*, *road speed*) used for determining the function for arterial roads were (1, 45), (2,35), (3, 25) and (4, 15).

Table S3 Road speed (unit in km h⁻¹) of different road type corresponded to the congestion levels

| Color | Congestion index range | Speed range (km h ⁻¹) | | |
|--------|------------------------|-----------------------------------|----------------|--------------------|
| | | Expressways | Arterial roads | Sub-arterial roads |
| Grey | 0-1 | >65 | 45 | >35 |
| | 1-2 | 50-65 | 35-45 | 25-35 |
| | 2-3 | 35-50 | 25-35 | 15-25 |
| Yellow | 3-4 | 20-35 | 15-25 | 10-15 |
| Red | 4-5 | <20 | <15 | <10 |

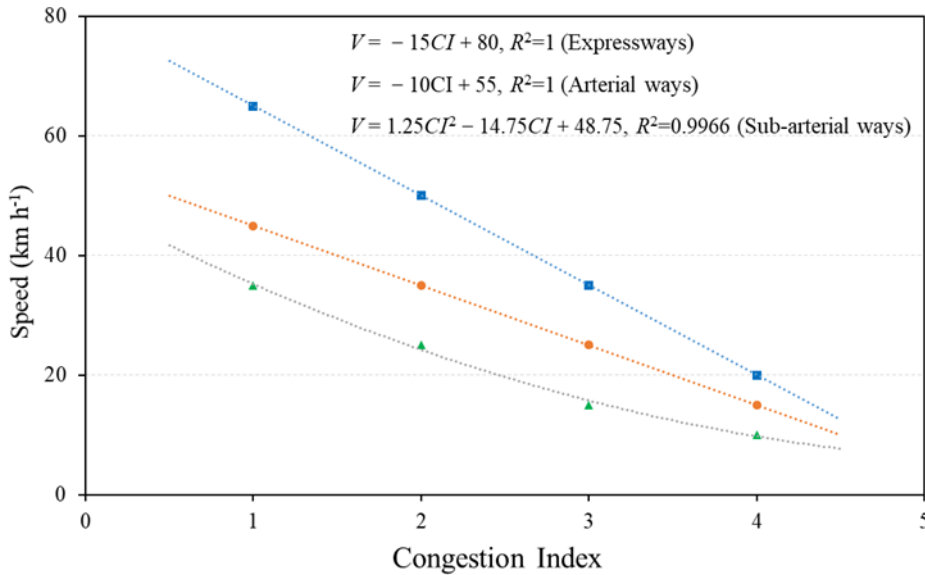


Figure S10. The relationships between the speed and the congestion index of different road types.

The original congestion map was updated every 5 mins. However, the color indicator embodies a large uncertainty in estimating road speed for that short episode (e.g., grey color indicates average speed greater than 20 km h⁻¹ for arterial roads). To reduce the uncertainty, we used the midpoint of congestion index range to digitalize the color indicator (e.g., 1.5 for grey, 3.5 for yellow and 4.5 for red) and aggregated 12 color indicators (i.e., proxy instantaneous congestion indexes) into an hourly average index for all the road segments included in the congestion map. We applied the relationship between congestion index and

road speed to derive hourly speeds in the research domain through the daytime (6:00 to 23:00 GMT+8). Fig. S11 provided an example of the entire process regarding speed estimation. The official website also reported average speeds (excluding minor roads) in various zones of Beijing during rush hours. As Fig. S12 indicates, the estimated average speeds in this study were close to the corresponding speeds reported by the official website on the annual level. As yellow and red indicators were rarely reported during nighttime (23:00 to 6:00 GMT+8), using the relationship functions in Fig. S10 would lead to underestimated road speeds. We referred to real-world nighttime vehicle speed data to calibrate our model, which were obtained from another project regarding large-scale GPS trajectory data collection from personal vehicles in Beijing (He et al., 2016).

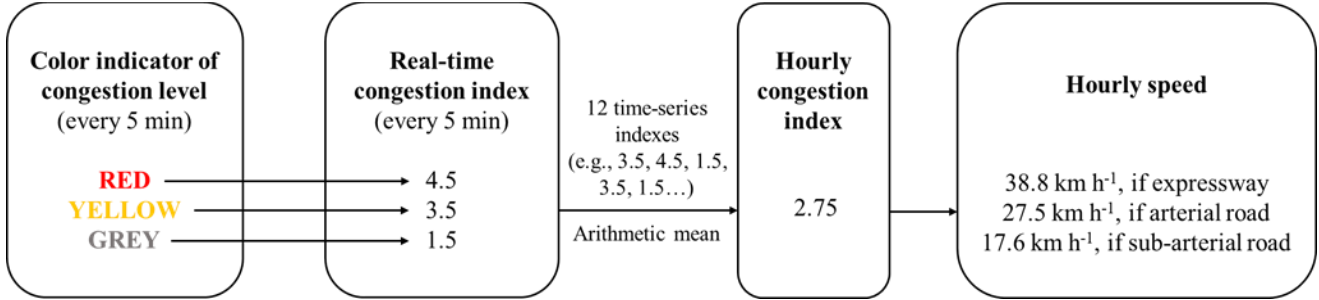


Figure S11. An example of the entire process regarding speed estimation

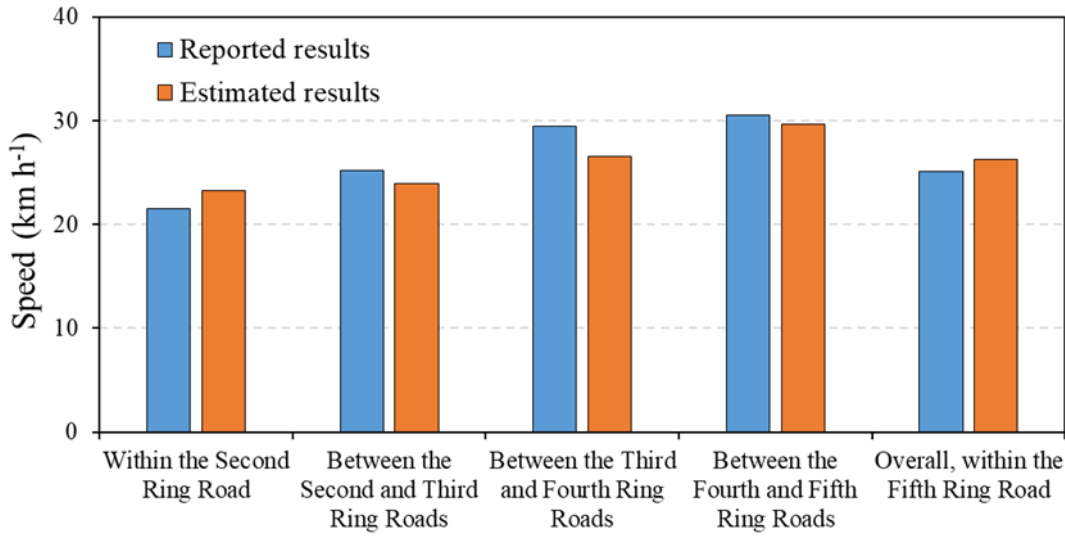


Figure S12. Comparison between estimated and reported speeds for evening rush hours of weekdays.

2.2 Localized traffic density functions

Local traffic density functions for expressways and arterial roads were developed based on annual average hourly traffic volume and speed data. 45 expressways and 12 arterial roads (hourly average single lane volumes ranged between 800 to 1500 veh h⁻¹) were used in this study, as road speed data were not available from other roads. We compared the fitting performance between two common traffic density models, i.e., Underwood and Greenshields functions. As Table S4 indicates, both models could nicely fit the arterial way group. For expressways, the fitting performance of Underwood model is better than Greenshields. For each road with available annual-average traffic volume, the dynamic traffic volume according to traffic congestion index informed speed is estimate according to Eq. (S2).

$$TV_{h,l} = \frac{Underwood(V_{h,l})}{Underwood(V_{0,h,l})} \cdot TV_{0,h,l} \quad (S2)$$

where $TV_{0,h,l}$ and $V_{0,h,l}$ are annual-average hourly traffic volume and speed for hour h and road link l , unit in veh h^{-1} and km h^{-1} , respectively; $TV_{h,l}$ is estimated traffic volume in response to traffic congestion index informed speed $V_{h,l}$ unit in veh h^{-1} and km h^{-1} , respectively.

Table S4 Comparison of model fitness of the localized empirical traffic density model in Beijing urban area

| Road type | Model functions | R^2 | NMB ^a | MFE ^b |
|---------------|---|-------|------------------|------------------|
| Expressways | Underwood: $q = 46.91u \ln(\frac{85.81}{u})$ | 0.50 | -0.16% | 21.9% |
| | Greenshields: $q = 71.12u(1 - \frac{u}{79.88})$ | 0.40 | -1.07% | 24.9% |
| Arterial ways | Underwood: $q = 46.17u \ln(\frac{54.34}{u})$ | 0.90 | 0.11% | 7.85% |
| | Greenshields: $q = 68.50u(1 - \frac{u}{51.13})$ | 0.90 | -0.16% | 8.54% |

Notes: ^a normalized mean bias; ^b mean fractional error.

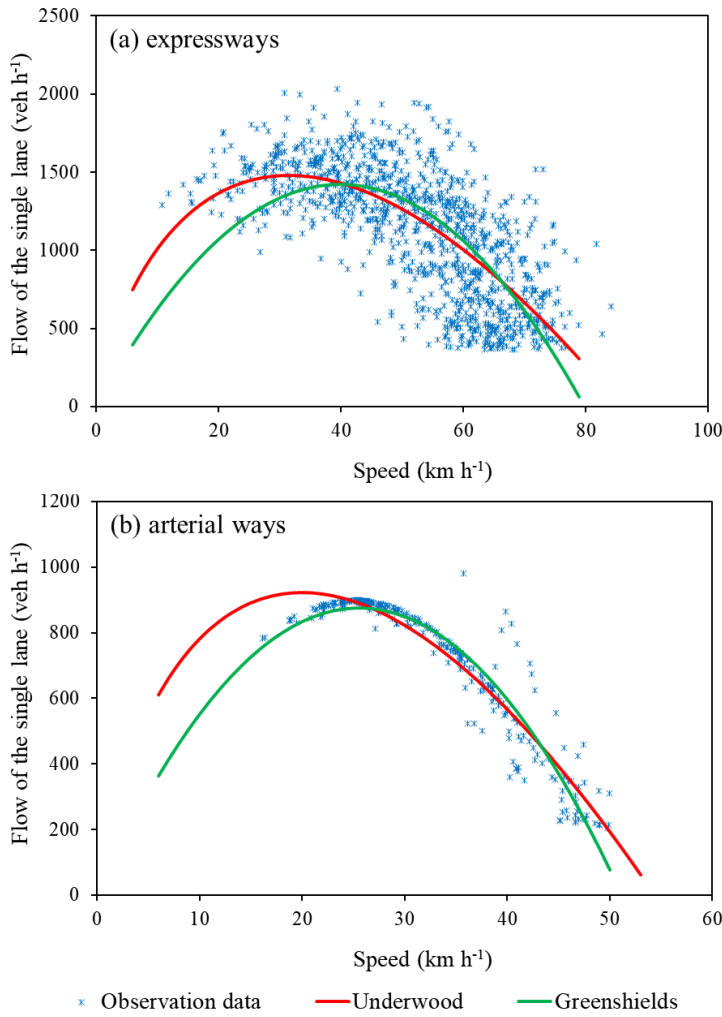


Figure S13. The localized empirical traffic density models developed based on the observation data: (a) expressways and (b) arterial ways.

2.3 Estimating traffic activities for nonmonitored roads

Traffic monitoring data (e.g., congestion index, annual traffic data, and intercity highway traffic monitoring) were not available for mostly minor roads and suburb/rural roads. We estimated traffic activities for these nonmonitored roads based on the average traffic data of monitored roads in the same corresponding traffic zone (see Fig. S14) and suggested volume/speed ratios between various road types (see Eq. S3).

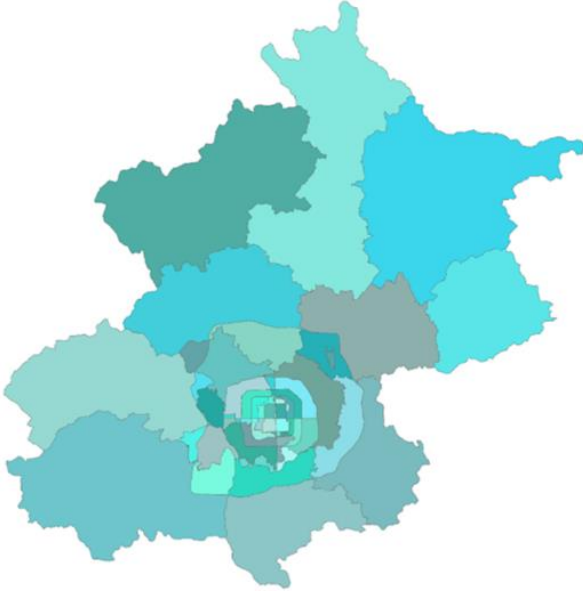


Figure S14. The map of traffic zones in Beijing

$$f_{n,i,k,j} = F_{i,j} \times \alpha_{k,i,j} \times m_n$$

(S3)

where $f_{n,i,k,j}$ is the traffic volume of the road link n with road type k in the traffic zone i at hour j , unit in veh h⁻¹; $F_{i,j}$ is the average single-line traffic volume of monitored baseline roads in traffic zone i at hour j , unit in veh h⁻¹; $\alpha_{k,i,j}$ is the traffic volume with the road type k in proportion to the average volume of baseline expressways in the traffic zone i at hour j (See Table S5); m_n is the number of lanes of the road number n . The suggested traffic volume ratios were reported by Beijing Jiaotong University, and summarized in Table S5.

Table S5 Single-lane traffic volume ratios of non-monitored roads to expressways (BJTU and Beijing EPB, 2014)

| Hour | Within the Sixth Ring Road | | | Outside the Sixth Ring Road | | |
|------|----------------------------|--------------------|-------------------|-----------------------------|--------------------|-------------------|
| | Arterial roads | Sub-arterial roads | Residential roads | Arterial roads | Sub-arterial roads | Residential roads |
| 0 | 49% | 28% | 29% | 12% | 7% | 7% |
| 1 | 50% | 30% | 25% | 12% | 8% | 6% |
| 2 | 45% | 24% | 20% | 11% | 6% | 5% |
| 3 | 41% | 22% | 21% | 10% | 6% | 5% |
| 4 | 37% | 20% | 16% | 9% | 5% | 4% |
| 5 | 36% | 24% | 25% | 9% | 6% | 6% |
| 6 | 42% | 29% | 33% | 10% | 7% | 8% |
| 7 | 43% | 31% | 42% | 11% | 8% | 11% |
| 8 | 42% | 33% | 33% | 11% | 8% | 8% |
| 9 | 41% | 32% | 29% | 10% | 8% | 7% |
| 10 | 42% | 33% | 30% | 10% | 8% | 7% |
| 11 | 40% | 32% | 29% | 10% | 8% | 7% |
| 12 | 40% | 32% | 28% | 10% | 8% | 7% |
| 13 | 41% | 33% | 33% | 10% | 8% | 8% |
| 14 | 35% | 32% | 26% | 9% | 8% | 7% |
| 15 | 41% | 32% | 28% | 10% | 8% | 7% |
| 16 | 42% | 34% | 29% | 10% | 8% | 7% |
| 17 | 46% | 36% | 30% | 11% | 9% | 7% |
| 18 | 44% | 33% | 27% | 11% | 8% | 7% |
| 19 | 39% | 30% | 26% | 10% | 8% | 6% |
| 20 | 39% | 31% | 25% | 10% | 8% | 6% |
| 21 | 39% | 31% | 25% | 10% | 8% | 6% |
| 22 | 40% | 30% | 26% | 10% | 7% | 6% |
| 23 | 46% | 29% | 24% | 11% | 7% | 6% |

Similarly, we estimated road average speeds for nonmonitored roads according to Eq. (S4).

$$\bar{v}_{n,k,i,j} = V_{i,j} \times \beta_{k,j,i} \quad (S4)$$

where $v_{n,i,j,k}$ is the traffic speed of the road number n with road type k in the traffic zone i at hour j , unit in km h^{-1} ; $V_{i,j}$ is the basic traffic speed of traffic zone i at hour j , unit in veh h^{-1} ; $\beta_{k,i,j}$ is the traffic speed with the road type k in proportion to the average speed of expressways in the traffic zone i at hour j . The speed ratios were derived based on trajectory data collected from nearly 500 personal vehicles in Beijing (He et al., 2016).

Part III. Simulating vehicular NO_x concentrations by using the RapidAir® model

Concentrations were modelled at 10m spatial resolution over the entire municipality of Beijing (16410 km^2). Hourly vehicular emissions of NO_x from all road links were used as linear emission input data. The RapidAir® model spatially allocates emissions to line sources at the desired resolution (i.e., 10m). For the city-level simulations, we didn't include localized high-resolution terrain and building profiles in the RapidAir modelling (i.e., default urban setting used). Meteorological profiles (surface and upper air measurement data) are download from National Oceanic and Atmospheric Administration (NOAA), including temperature, wind speed, wind direction distribution, cloud coverage, etc. for the surface, as well as the temperature, atmospheric pressure, wind speed, etc. for upper air. Major surface and upper air meteorology sites for Beijing are No. 545110 and No. 54511, which are located at the Beijing International Airport. Additionally, two extra sites (544,050 at Huailai and 545,273 at Tianjin) in surrounding cities were referred to for some outlying areas in Beijing. Fig. S15 illustrates the annual-average hourly temperature and wind speed profiles. Fig. S16 presents the average daytime and nighttime wind rose maps to indicate the frequency of wind direction. Surface parameters (Bowen, Rough, Albedo) are set according to the AERMOD user guidebook (USEPA, 2018), respectively set as $B = 2.0$, $R = 0.3$, and $A = 0.25$. For the Gaussian plume in the dispersion model, there are some major parameters set according to further experience in city modelling, e.g. receptor height = 1.5 m; Release height = 1.4m; Initial depth = 1.0m.

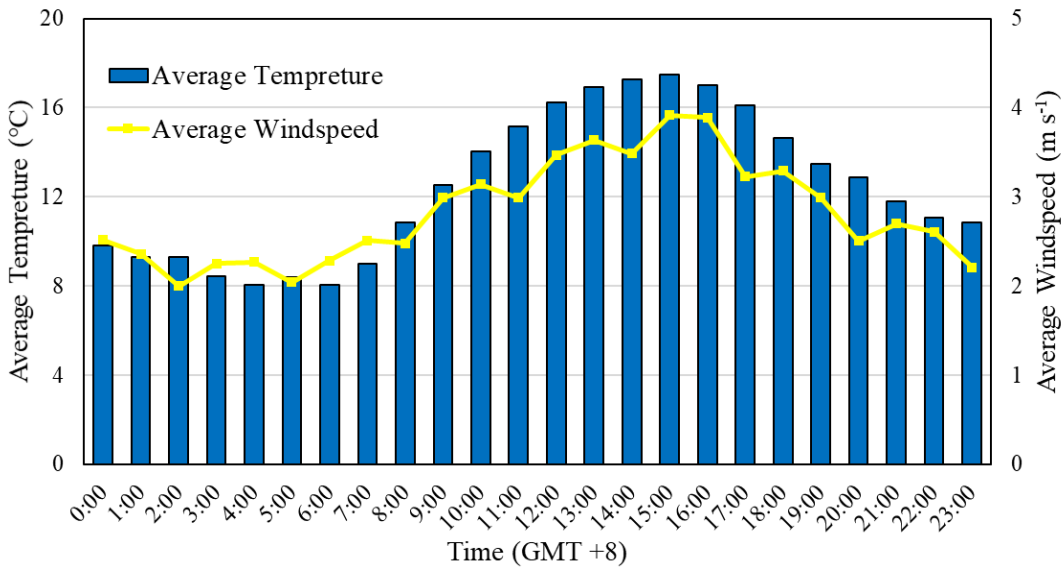


Figure S15. Annual-average hourly temperatures and wind speeds.

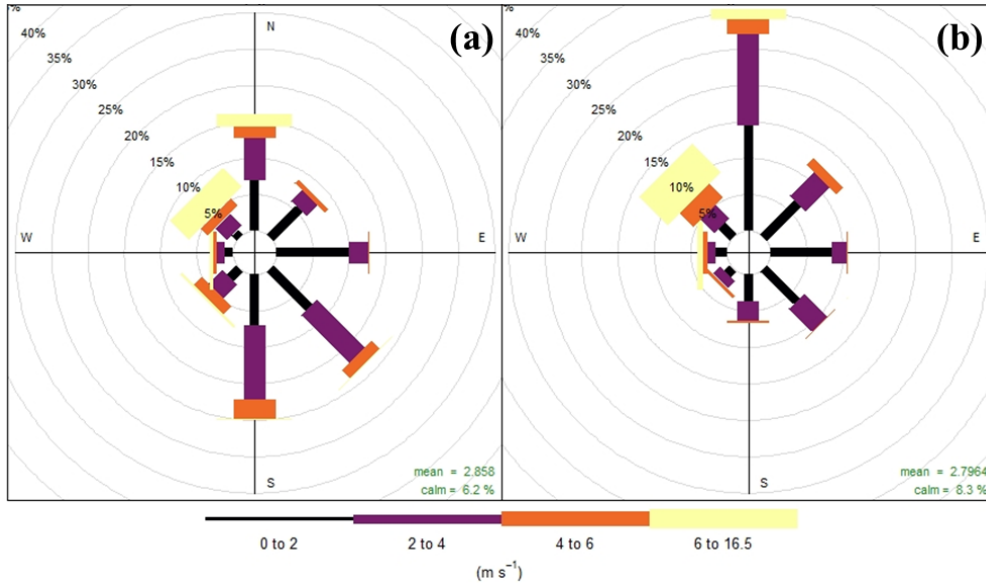


Figure S16. Average wind direction patterns for (a) daytime (6:00 to 22:00 GMT+8) and (b) nighttime (23:00 to 6:00 GMT+8), respectively. The nighttime meteorological profiles were used to estimate the environmental impacts from the nighttime use of trucks in Beijing.

For the fine-grained hotspot simulations (gridded spatial resolution at 1 m×1m), additional data are applied to improve the accuracy. First, the number of traffic lanes for each road has been specified, which further design the emission sources as multiple parallel lines (e.g., more than 10 lines for the major expressways in each hotspot domain, including the side road segments). Second, the profiles of building profiles are required to estimate the street canyon effect. The detailed methodology (based on the AEOLIUS model developed by the UK Meteorological Office) and evaluation of using geospatial surrogates to represent street canyon effects have been reported by Masey et al. (2018) (Masey et al., 2018). The buildings and height data were derived from OpenStreetMap and observation, traffic volume and speed data were from emission inventory. Figure S17 uses yellow area to represent the street canyon domains identified by the RapidAir®. Furthermore, the concentration gradients across major expressways (A) and arterial roads (B) in two hotspot regions are also summarized in Fig. S17.

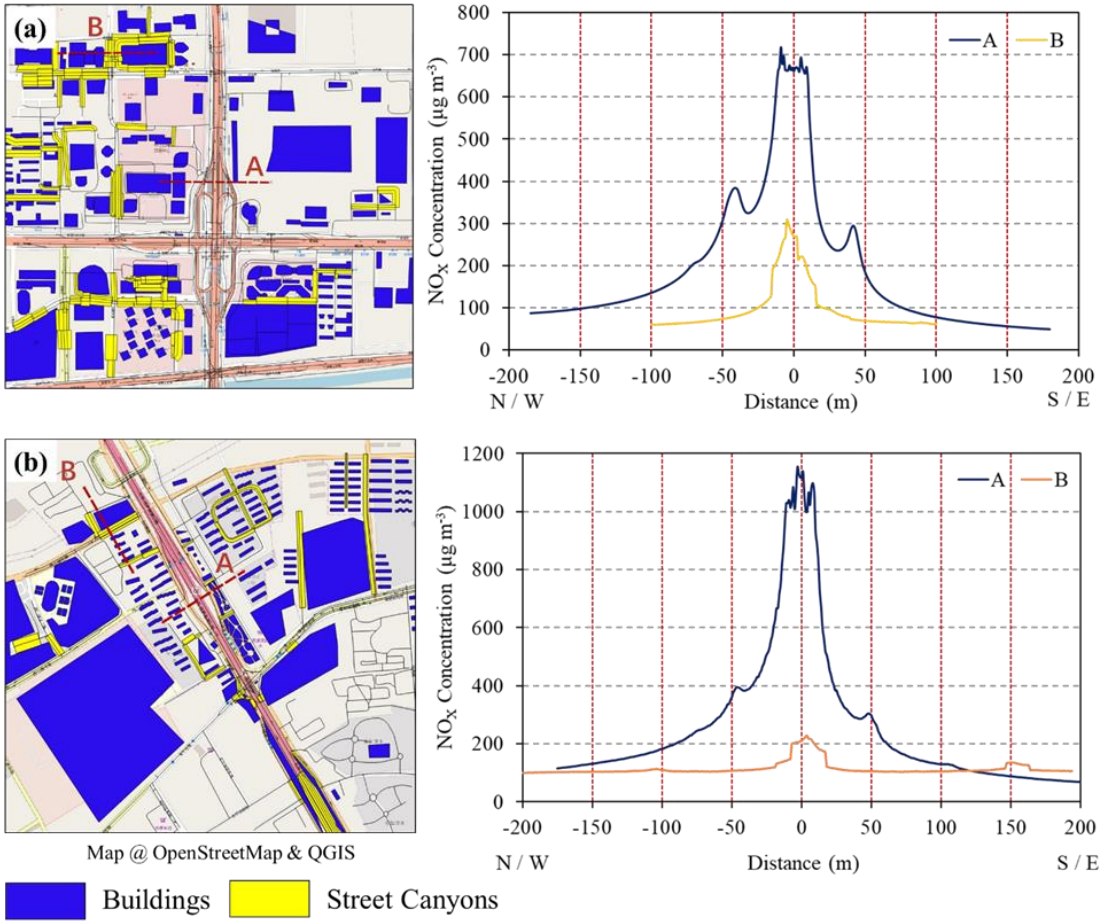
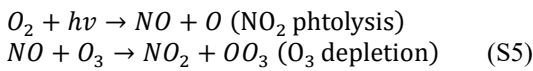


Figure S17. Maps and cross-road NO_x concentrations for two hotspot regions: (a) Guomao and (b) Xisanqi.

We compared the simulated NO_x concentrations and the observed results from official air quality monitoring sites in Beijing (12 urban environment sites all located within the Sixth Ring Road and 5 urban traffic sites). We referred to site-specific cells in the RapidAir® results to derived the simulated vehicular NO_x concentrations. However, only NO₂ data rather than NO_x (i.e., separate NO₂ and NO concentrations) are reported to the public in China. To crossover the barrier, we referred to the approximate photostationary state and established a chemical equilibrium for NO₂ between the NO₂ photolysis and the O₃ depletion (important reactions), which was applied to estimate site-specific NO concentrations (See Eq. S5). We constrain the comparison within the daytime time framework (6:00 to 18:00 GMT+8) in 2013. The nighttime simulations have not been included because of the complicated nighttime NO_x chemistry.



Then the NO concentration is estimated according to the reaction rate constants of NO₂ photolysis (J , solar radiation dependent) and O₃ depletion (k , temperature dependent), NO₂ and O₃ concentrations (see Eq. S6)

$$[NO]_i = \frac{J[NO_2]_i}{k[O_3]_i} \quad (S6)$$

where $[NO]_i$, $[NO_2]_i$, and $[O_3]_i$ are annual-average daytime concentrations of NO (estimated), NO₂ (official observation) and O₃ (official observation) at site i (converted in ppbv); J and k are the average reaction rate constants, $4.7 \times 10^{-3} \text{ s}^{-1}$ (average solar radiation of 311 W/m) (Trebs et al., 2009; NASA, 2018; Zou et al., 2016) and $4.5 \times 10^{-4} \text{ s}^{-1} \text{ ppbv}^{-1}$ (average daytime temperature at 287 K) (NASA and JPL, 2015), respectively. Then, the total NO_x concentrations are estimated as the sum of observed NO₂ and estimated NO.

Part IV. Comparing emission inventories based on link-level traffic data and top-down allocation methods

M2: Allocation based on population distribution. M2 utilized GIS grid-based population densities as spatial surrogates to allocate total emissions, which equaled the total emissions based on link-level traffic profiles (i.e., M1). The population data meshed into 1 km × 1 km cells were obtained from the LandScan 2012 (ORNL, 2012). For each cell j , allocated vehicle emissions were estimated with Eq. S7.

$$E_{M2\ j,p} = \frac{E_p}{TP} P_j \quad (S7)$$

where $E_{M2\ j,p}$ is the allocated emissions of air pollutant p in cell j ; E_p is total emissions of air pollutant p estimated according to M1; TP is the total population of the entire municipality of Beijing; P_j is the population in the grid cell j .

M3: Allocation based on road length and type. Eq. S8 illustrates the way to allocate vehicle emissions according to total standard road length in each cell.

$$E_{M3\ j,p} = \frac{E_p}{\sum_k UL_k \cdot UW_k + \sum_k RL_k \cdot RW_k} \times (\sum_k UL_{j,k} \cdot UW_k + \sum_k RL_{j,k} \cdot RW_k) \quad (S8)$$

where $E_{M3\ j,p}$ is the allocated vehicle emissions of air pollutant p in cell j ; UL_k and RL_k represent the total actual road length of the road type k in the urban (including the area between Fifth Ring Road and Sixth Ring Road) and suburb/rural areas (outside Sixth Ring Road), respectively; $UL_{j,k}$ and $RL_{j,k}$ represent the actual road length of the road type k in grid cell j , respectively; UW_k and RW_k are coefficients to estimate standard road length (e.g., $UL_{j,k} \cdot UW_k$ or $RL_{j,k} \cdot RW_k$), which were defined by area and road type.

UW and RW represent weighting factors of traffic volumes by region and road type, which were estimated according to Eq. S9.

$$\begin{aligned} UW_k &= R_u \frac{m_k \alpha_{Uk}}{\sum_k m_k \alpha_{Uk}} \\ RW_k &= R_r \frac{m_k \alpha_{Rk}}{\sum_k m_k \alpha_{Rk}} \end{aligned} \quad (S9)$$

where R_u and R_r are the traffic volume ratio of two defined regions to the total traffic volumes of the entire Beijing ($R_u=0.8$ and $R_r=0.2$, here with reference to the traffic pattern results of M1); m_k is the number of the lanes; and α_{Uk} and α_{Rk} are the traffic volume proportions of different road types to expressways in Table S5.

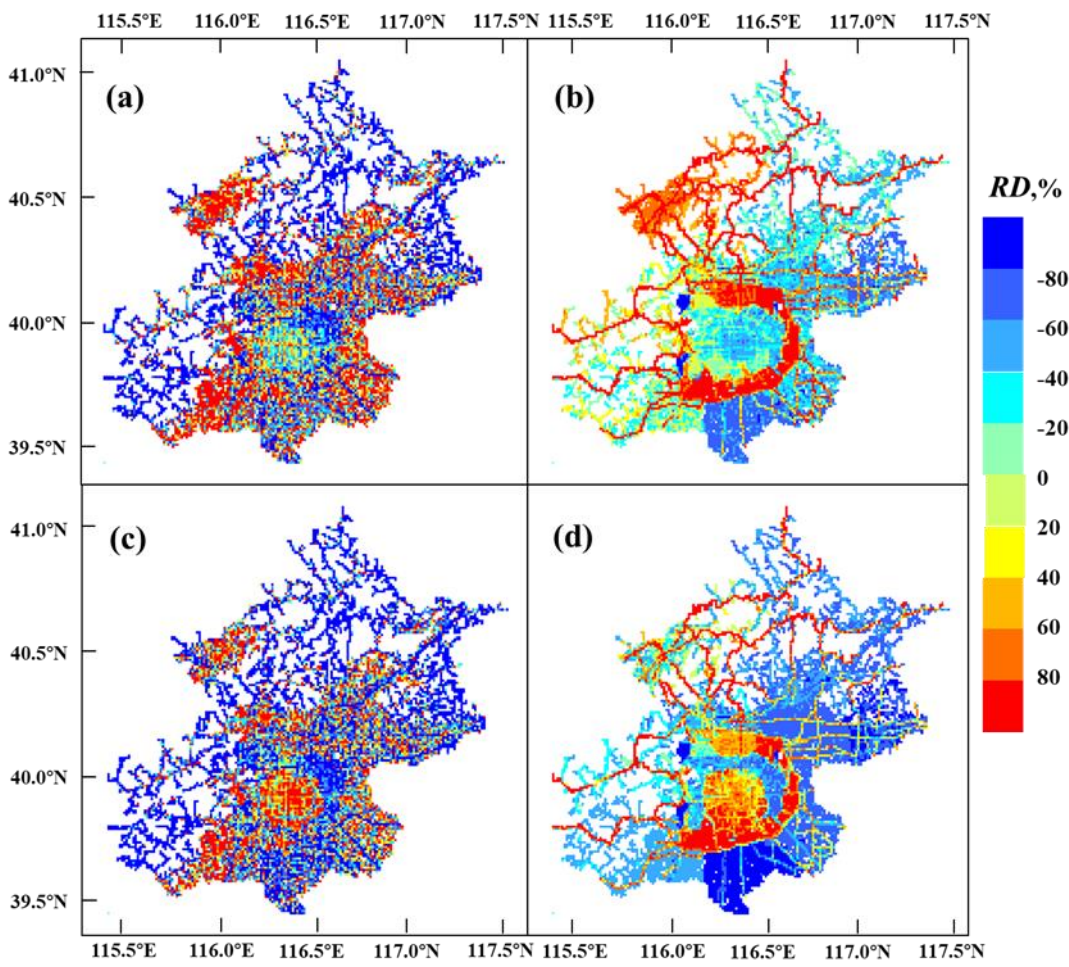


Figure. S18 Spatial distributions of relative discrepancies (RD) of CO (a, M2 vs. M1; b, M3 vs. M1) and BC (c, M2 vs. M1; d, M3 vs. M1) emissions by using various methods

References

- Beijing Jiaotong University (BJTU) and Beijing Environmental Protection Bureau (Beijing EPB), Research on the improvement on the decision system of vehicle emission control (in Chinese), Beijing EPB, Beijing, P. R. China, 2014.
- Beijing Municipal Administration of Quality and Technology Supervision and Beijing Transport Institute (BTI), The evaluation system of the congestion of the urban roads (DB11/T 785-2011) (in Chinese), Beijing Transport Institute, Beijing, P. R. China, 2011.
- He, X., Wu, Y., Zhang, S., Tamor, M. A., Wallington, T. J., Shen, W., Han, W., Fu, L., and Hao, J.: Individual trip chain distributions for passenger cars: Implications for market acceptance of battery electric vehicles and energy consumption by plug-in hybrid electric vehicles, *Applied Energy*, 180, 650-660, 10.1016/j.apenergy.2016.08.021, 2016.
- National Aeronautics and Space Administration (NASA): EarthData: Calibrated Radiance and Solar Radiance, 2018 (accessed). Available at <https://earthdata.nasa.gov/discipline/radiance>
- National Aeronautics and Space Administration (NASA) and Jet Propulsion Laboratory (JPL): Chemical Kinetics and Photochemical Data for Use in Atmospheric Studies, Evaluation Number 18 (JPL Publication 15-10), 2015. Available at https://jpldataeval.jpl.nasa.gov/pdf/JPL_Publication_15-10.pdf
- Masey, N., Hamilton, S., and Beverland, I. J.: Development and evaluation of the RapidAir® dispersion model, including the use of geospatial surrogates to represent street canyon effects, *Environmental Modelling & Software*, 2018.
- Oak Ridge National Laboratory (ORNL): LandScan Global Population Database, Oak Ridge National Laboratory, Oak Ridge, Tenn., USA, 2012.
- Trebs, I., Bohn, B., Ammann, C., Rummel, U., Blumthaler, M., Königstedt, R., Meixner, F., Fan, S., and Andreae, M.: Relationship between the NO₂ photolysis frequency and the solar global irradiance, *Atmospheric Measurement Techniques*, 2, 725-739, 2009.
- USEPA, User's Guide for the AMS/EPA Regulatory Model – AERMOD. EPA-454/B-18-001. U.S. Environmental Protection Agency, Research Triangle Park, NC. 1, 2018. Available at <https://www.epa.gov/scram/>.
- Wu, Y., Zhang, S., Li, M., Ge, Y., Shu, J., Zhou, Y., Xu, Y., Hu, J., Liu, H., and Fu, L.: The challenge to NO_x emission control for heavy-duty diesel vehicles in China, *Atmospheric Chemistry and Physics*, 12, 9365-9379, 2012.
- Zhang, S., Wu, Y., Wu, X., Li, M., Ge, Y., Liang, B., Xu, Y., Zhou, Y., Liu, H., Fu, L., and Hao, J.: Historic and future trends of vehicle emissions in Beijing, 1998–2020: A policy assessment for the most stringent vehicle emission control program in China, *Atmospheric Environment*, 89, 216-229, 10.1016/j.atmosenv.2013.12.002, 2014.
- Zhang, S., Niu, T., Wu, Y., Zhang, K. M., Wallington, T. J., Xie, Q., Wu, X., and Xu, H.: Fine-grained vehicle emission management using intelligent transportation system data, *Environmental Pollution*, 241, 1027-1037, 10.1016/j.envpol.2018.06.016, 2018.
- Zou, Q., Lu, K., Wu, Y., Yang, Y., Du, Z., and Hu, M.: Ambient photolysis frequency of NO₂ determined using chemical actinometer and spectroradiometer at an urban site in Beijing, *Frontiers of Environmental Science & Engineering*, 10(6), 13, 10.1007/s11783-016-0885-3, 2016